Force Schemes in Simulations of Granular Materials

J. Shäfer, S. Dippel, D. Wolf

▶ **To cite this version:**

J. Shäfer, S. Dippel, D. Wolf. Force Schemes in Simulations of Granular Materials. Journal de Physique I, 1996, 6 (1), pp.5-20. 10.1051/jp1:1996129 . jpa-00247176

HAL Id: jpa-00247176
https://hal.science/jpa-00247176v1

Submitted on 4 Feb 2008

HAL is a multi-disciplinary open access archive for the deposit and dissemination of scientific research documents, whether they are published or not. The documents may come from teaching and research institutions in France or abroad, or from public or private research centers.

L'archive ouverte pluridisciplinaire **HAL**, est destinée au dépôt et à la diffusion de documents scientifiques de niveau recherche, publiés ou non, émanant des établissements d'enseignement et de recherche français ou étrangers, des laboratoires publics ou privés.

Force Schemes in Simulations of Granular Materials

J. Schäfer(*), S. Dippel and D. E. Wolf

Höchstleistungsrechenzentrum, Forschungszentrum Jülich, D-52425 Jülich, Germany

(Received 3 July 1995, received in final form and accepted 12 October 1995)

Abstract. — In computer simulations of granular flow, one widely used technique is classical soft-sphere Molecular Dynamics, where the equations of motion of the particles are numerically integrated. This requires specification of the forces acting between grains. In this paper, we systematically study the properties of the force laws most commonly used and compare them with recent experiments on the impact of spheres. We point out possible problems and give criteria for the right choice of parameters. Finally, two generic problems of soft-sphere simulations are discussed.

PACS. 07.05Tp – Computer modeling and simulation.
PACS. 46.30Pa – Friction, wear, adherence, hardness, mechanical contacts, and tribology.
PACS. 83.70Fn – Granular solids.

1. Introduction

Flows of granular materials are ubiquitous in industry and nature. Despite their technological importance, their properties (among which are size segregation [1,2], sudden transitions from flowing to sticking [3], density waves [4,5] and "silo music" [6]) are far from well understood. Computer simulations have turned out to be a powerful tool to investigate the physics of granular flow, especially valuable as there is no generally accepted theory of granular flow so far, and experimental difficulties are considerable. A very popular simulation scheme is an adaptation of the classical Molecular Dynamics technique. It consists of integrating Newton's equations of motion for a system of "soft" grains starting from a given initial configuration. This requires giving an explicit expression for the forces that act between grains. In principle, contact mechanics should provide such expressions, but the problem of two touching bodies under general conditions is very complicated (see, e.g., [7] and references therein). Many more or less strongly simplified force schemes have thus been suggested and employed in simulations (e.g., [8–20]), often without a thorough discussion of their properties.

The aim of the present paper is three-fold: firstly, to give a brief account of theoretical considerations and experimental results concerning the free impact of spheres; secondly, to critically compare the properties of existing force schemes on these grounds, and to give hints on their correct use; and thirdly, to discuss some generic problems that can occur in soft sphere simulations independently of the force laws used. We perform example simulations to illustrate the properties of the force laws with a constant-timestep fifth order predictor-corrector algorithm [21]. Although it is in principle desirable to work with non-dimensional units, they

(*) Permanent address: FB 10, Theoretical Physics, Gerhard Mercator University, D-47048 Duisburg, Germany; e-mail: j.schaefer@kfa-juelich.de

© Les Éditions de Physique 1996

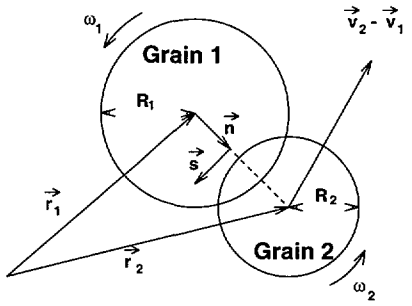

Fig. 1. — Definition of the quantities used for description of the impact.

are not always practical; for example, non-linear force laws do not define a unique timescale, as will be discussed later. Therefore, we decided to use SI units, and tuned all parameters such as to mimic a specific granular material, namely the cellulose acetate spheres used in experiments by Drake [22–24] and Foerster *et al.* [25], of radius $R = 3$ mm and mass $m = 1.48 \times 10^{-4}$ kg. Thus, we are able to compare our simulation results directly to experimental data [25].

We limit ourselves to the case of non-cohesive, dry, spherical grains which are restricted to three degrees of freedom (two translational, one rotational), as would be the case in a two-dimensional setup. A general contact between two grains of radii R_i, positions $\mathbf{r}_i$, velocities $\mathbf{v}_i$, and angular velocities ω_i $(i = 1, 2)$ is sketched in Figure 1. The deformation of the grains is parametrized by the "virtual overlap" ξ,

$$\xi = \max\,(0,\, R_1 + R_2 - |\mathbf{r}_2 - \mathbf{r}_1|).$$

Two unit vectors $\mathbf{n}$ and $\mathbf{s}$ are used to decompose the forces and velocities into normal and shear components:

$$\begin{aligned} \mathbf{n} &= \frac{\mathbf{r}_2 - \mathbf{r}_1}{|\mathbf{r}_2 - \mathbf{r}_1|} = (n_x, n_y) \\ \mathbf{s} &= (n_y, -n_x). \end{aligned}$$

Thus, the relative normal velocity v_n and relative shear velocity v_s are given by

$$\begin{aligned} v_n &= (\mathbf{v}_2 - \mathbf{v}_1) \cdot \mathbf{n} \\ v_s &= (\mathbf{v}_2 - \mathbf{v}_1) \cdot \mathbf{s} + \omega_1 R_1 + \omega_2 R_2. \end{aligned}$$

If the shear velocity component v_s is equal to zero at the beginning of a contact, the impact is head on or *normal*, otherwise it is shearing or *oblique*. We begin our discussion in Section 2 with normal impacts introducing the normal force F_n, and proceed to oblique impacts and the shear force F_s in Section 3.

2. Normal Impacts

In general, two colliding spheres undergo a deformation which will be somewhere between the extremes of perfectly inelastic and perfectly elastic. Possible mechanisms for dissipation (i.e., transformation of kinetic energy into other forms of energy which ultimately transform into heat) are [7] plastic deformation, viscoelasticity of the material, and also elastic waves excited

by the impact. The latter are always present — they make the noise — but carry so little energy that one can generally neglect them as source of dissipation. Phenomenologically, the elasticity of the impact is described by the coefficient of normal restitution e_n,

$$e_n = -v_n^{\mathrm{f}}/v_n^{\mathrm{i}} \in [0,1].$$

Here and in the following, the superscript i refers to pre-collisional (initial) and f to post-collisional (final) quantities.

According to Johnson [7], the necessary critical yield velocity causing plastic deformation is given by

$$v_{\mathrm{yield}}^2 \approx 107 \frac{R_{\mathrm{eff}}^3}{m_{\mathrm{eff}}} \frac{Y^5}{E_{\mathrm{eff}}^4} \tag{1}$$

where $m_{\mathrm{eff}} = (m_1 m_2)/(m_1+m_2)$ and $R_{\mathrm{eff}} = (R_1 R_2)/(R_1+R_2)$ are the reduced mass and radius, Y is the yield strength of the softer of the spheres, and E_{eff} is related to Young's modulus E and Poisson's ratio ν of both spheres through $1/E_{\mathrm{eff}} = (1-\nu_1^2)/E_1 + (1-\nu_2^2)/E_2$. If $v_n^{\mathrm{i}} < v_{\mathrm{yield}}$, no plastic deformation may occur during the impact, and all energy loss should be due to viscoelasticity. If $v_n^{\mathrm{i}} > v_{\mathrm{yield}}$, on the other hand, the energy loss due to plastic deformation must dominate over the energy loss due to viscoelasticity. Most materials have a critical yield velocity that is quite small (e.g. $v_{\mathrm{yield}} \approx 0.14$ m/s for cellulose acetate, $v_{\mathrm{yield}} \approx 0.02$ m/s for steel).

For the case of plastic deformation, a simple theory [7] predicts e_n to fall off like ${v_n^{\mathrm{i}}}^{-1/4}$ with increasing impact velocity. For the case of purely viscoelastic losses, Kuwabara and Kono [26] obtain a coefficient of normal restitution e_n that also decreases with increasing v_n^{i}; for e_n close to one, $(1-e_n) \propto {v_n^{\mathrm{i}}}^{1/5}$ Experimental studies by Goldsmith and others [27], Bridges *et al.* [28], Kuwabara and Kono [26] and Sondergaard *et al.* [29] for spheres made of a large class of different materials all show a slight monotonic decrease of e_n with increasing v_n^{i} which is compatible with a ${v_n^{\mathrm{i}}}^{-1/4}$ power law over several orders of magnitude of v_n^{i}. On the other hand, measurements by Drake and Shreve [22] and Foerster *et al.* [25] on cellulose acetate spheres show no systematic dependence of e_n on v_n^{i} for the range of impact velocities used, which in both cases was rather narrow (Foerster *et al.* measured $e_n \approx 0.87$ in a velocity range $0.29\ \mathrm{m/s} \leq v_n^{\mathrm{i}} \leq 1.2\ \mathrm{m/s}$).

Modelling a force that leads to inelastic collisions requires at least two terms: repulsion and some sort of dissipation. The simplest force with the desired properties is the damped harmonic oscillator force

$$F_n = -k_n \xi - \gamma_n \dot{\xi}, \tag{2}$$

where γ_n is a damping constant and k_n is related to the stiffness of a spring whose elongation is ξ, the deformation of the grain. This model (also referred to as *linear spring-dashpot*) has the advantage that its analytic solution (with initial conditions $\xi(0) = 0$ and $\dot{\xi}(0) = v_n^{\mathrm{i}}$) allows the calculation of important quantities. For instance, the coefficient of normal restitution is

$$e_n = \exp\left(-\frac{\gamma_n}{2m_{\mathrm{eff}}} t_n\right), \tag{3}$$

where

$$t_n = \pi \left(\frac{k_n}{m_{\mathrm{eff}}} - \left(\frac{\gamma_n}{2m_{\mathrm{eff}}} \right)^2 \right)^{-1/2} \tag{4}$$

denotes the duration of the collision. The maximum overlap during a collision is

$$\xi_{\max} \leq v_n^{\mathrm{i}} t_n / \pi, \tag{5}$$

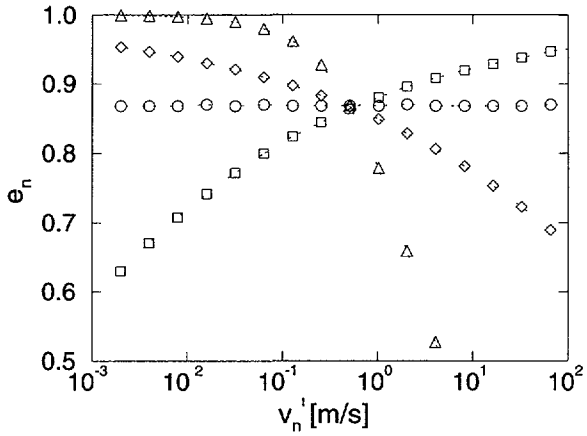

Fig. 2. — Dependence of coefficient of normal restitution e_n on the impact velocity v_n^i for various normal forces. (o) Linear spring-dashpot (2), (□) Hertz law with linear damping (8), (◇) Hertz-Kuwabara-Kono force (9), (△) Walton-Braun force (10).

where the equality holds for elastic grains ($e_n = 1$). An accurate simulation (reproducing the analytic e_n with relative errors of the order 10^{-4}) requires a constant time step $\Delta t \approx t_n/100$. In principle, force (2) has no free parameters, since k_n and γ_n can be set adjusting e_n and t_n to the corresponding experimental values exhibited by a given material in a velocity range relevant for the simulations. Because of its advantages, it has been used in numerous works [9–12, 15, 16, 30]. In Figure 2, its behaviour is illustrated for $e_n = 0.87$ and $t_n = 1 \times 10^{-5}$ s ($\Leftrightarrow k_n = 7.32 \times 10^6$ N/m, $\gamma_n = 2.06$ kg/s).

In order to formulate a more refined force than (2), one can use the results of the Hertz theory of elastic contact [7, 31, 32], which predicts the following repulsive force for the case of spheres:

$$F_n = -\tilde{k}_n \xi^{3/2} \tag{6}$$

Here, $\tilde{k}_n$ is a non-linear stiffness connected to the elastic properties and to the radii of the spheres through $\tilde{k}_n = 4/3\sqrt{R_{\text{eff}}}E_{\text{eff}}$. For Drake's cellulose acetate spheres, $\tilde{k}_n = 9.0 \times 10^7$ Nm$^{-3/2}$. Note that with (6), the collision time t_n is no longer independent of v_n^i [32]:

$$t_n = 3.21 \left(\frac{m_{\text{eff}}}{\tilde{k}_n}\right)^{2/5} {v_n^i}^{-1/5} \tag{7}$$

This means that there is no intrinsic timescale to collisions. The choice of the numerical time step Δt must depend on the maximum relative velocities expected during the simulation to ensure satisfactory numerical accuracy. In our simulations, we have a maximum impact velocity of about 100 m/s, for which $t_n \approx 1.88 \times 10^{-5}$ s, and we set $\Delta t = t_n/100$.

In order to obtain a *dissipative* Hertz-type force, a viscous damping term was added to the Hertz force in an *ad hoc* fashion in some studies [13, 17, 33]:

$$F_n = -\tilde{k}_n \xi^{3/2} - \gamma_n \dot{\xi}. \tag{8}$$

However, as Taguchi [34] pointed out, this force leads to collisions that become more elastic as the impact velocity increases, contrary to the experimental evidence: $(1 - e_n) \propto {v_n^i}^{-1/5}$ [35]. For low impact velocities, where the Hertz results for elastic contacts should be regained, force

(8) produces a coefficient of restitution that approaches zero. In Figure 2, we illustrate this behaviour using $\gamma_n = 0.35$ kg/s, so that $e_n \approx 0.87$ in the velocity range covered by Foerster's measurements [25].

Kuwabara and Kono [26] and Brilliantov *et al.* [36] extend the original Hertz approach assuming the material to be viscoelastic instead of elastic. They derive

$$F_n = -\tilde{k}_n \xi^{3/2} - \tilde{\gamma}_n \xi^{1/2} \dot{\xi}, \tag{9}$$

where $\tilde{k}_n$ is identical to the $\tilde{k}_n$ from Hertz theory and $\tilde{\gamma}_n$ is connected to the radii of the spheres and the two coefficients of bulk viscosity. This force leads to a coefficient of normal restitution e_n that decreases with increasing v_n^{i}, in agreement with experimental results: $(1 - e_n) \propto {v_n^{\mathrm{i}}}^{1/5}$ [26,35]. In Figure 2, we illustrate this using $\tilde{\gamma}_n = 190$ kg m$^{-1/2}$ s^{-1}.

An approach guided by the picture of plastic deformation was presented by Walton and Braun [37]. They assume that there are different spring constants, k_1 and k_2, for the loading and unloading part of the contact:

$$F_n = \begin{cases} k_1 \xi & , \quad \dot{\xi} \geq 0 \quad \text{(loading)} \\ k_2(\xi - \xi_0) & , \quad \dot{\xi} < 0 \quad \text{(unloading)} \end{cases} \tag{10}$$

where ξ_0 is the value of ξ where the unloading curve intersects the abscissa under the given circumstances, or the permanent plastic deformation. In this model, $e_n = \sqrt{k_1/k_2}$. By making k_2 a function of the maximum force $F_n^{\max}$ achieved during loading, $k_2 = k_1 + sF_n^{\max}$, e_n can be made a decreasing function of the impact velocity v_n^{i}, $e_n = (sv_n^{\mathrm{i}}(m_{\mathrm{eff}}/k_1)^{1/2} + 1)^{-1/2}$. In Figure 2, we illustrate this behaviour with $k_1 = 7.32 \times 10^6$ N/m and $s = 2 \times 10^5$ m^{-1}.

As a final remark, we want to comment on the use of the reduced mass m_{eff} in the forces (omitted here for simplicity). In some studies, it is understood as an additional prefactor for the damping term [10,11,13,14,17,18,30], leading to a coefficient of restitution that decreases with increasing m_{eff}. Other authors put it as prefactor in both the elastic and the dissipative term [15,16,34], such that the coefficient of restitution becomes independent of m_{eff}. If neither of the two terms is given a prefactor m_{eff} [8,9,12], e_n is an increasing function of m_{eff}. Unfortunately, there is no systematic experimental research on the mass dependence of e_n to our knowledge except some work dating from 1864, cited by Goldsmith [27], which indicates a slight decrease of e_n with increasing m_{eff} for spheres of equal size. This result suggests that the first of the possibilities described above might be most suited. It is definitely most desirable that more experimental work be done in order to settle this point. However, when the granular flow consists of particles without large mass differences, putting m_{eff} into the forces merely amounts to redefining the stiffness and /or damping constant.

3. Oblique Impacts and Frictional Contacts

We now turn to impacts where $v_s^{\mathrm{i}} \neq 0$, such that there is a non-vanishing tangential component of the force, or shear force for short. In general, the shear force is connected to the normal force by the Coulomb laws of friction, namely

$$F_s \leq \mu_{\mathrm{s}} F_n \quad \text{for static friction } (v_s = 0), \tag{11}$$

$$F_s = \mu_{\mathrm{d}} F_n \quad \text{for dynamic friction } (v_s \neq 0). \tag{12}$$

Here μ_{s} and μ_{d} are the coefficients of static and dynamic friction, respectively. The "$\leq$" sign in (11) means that for the case of static friction, F_s compensates exactly the (unknown) external

force F_s^{ext} applied to the contact, so that $v_s = 0$ is maintained. If $F_s^{\text{ext}} > \mu_s F_n$, one enters the dynamic friction regime and equation (12) applies. Normally, $\mu_s > \mu_d$ and both are about 0.5.

In the contact area of two colliding convex bodies, a *local* version of equations (11) and (12) relates the normal and the shear stresses along the contact. For elastically similar bodies, the shear stresses do not influence the normal stress distribution over the contact area [7], so that the results of Hertz theory can still be used for the normal stresses. Then, in the outer regions of the contact area, where the normal stresses are small because the strains are small, one must in general expect the condition for dynamic friction to be fulfilled, whereas in the central regions, where large normal strains and stresses are present, static friction may occur. This leads to the development of an *annulus of microslip* surrounding an inner *region of sticking* in the contact area. Because the friction laws are strongly nonlinear, the size and form of the annulus of microslip depend on the loading–unloading history of the contact, making the prediction of tangential deformation and friction forces, in a given situation, complicated [38]. Mindlin and Deresiewicz [39] have discussed the tangential friction forces between two elastic spheres for the case of several distinct loading-unloading histories and assuming the Hertz theory to hold. Maw *et al.* [40,41] and Walton [42] performed such an analysis for the case of the oblique impact of spheres. An interesting result is that due to the ability of the sticking contact to store and restore "tangential" kinetic energy, there may be a reversion of tangential velocity v_s under certain circumstances, a fact experimentally confirmed for discs [41] and spheres [25,27].

To illustrate the properties of the shear force laws discussed in the following, we implemented them and carried out test simulations of free binary impacts with varying obliqueness. We directly compare the results to the experimental results of [25]. The linear spring-dashpot force (2) was used as normal force in all cases, because it is simple, robust and, most importantely, makes the results of oblique impacts only dependent on the obliqueness, not on the absolute value of the impact velocity v_n^{i}. We adopt the values $e_n = 0.87$ ($\Leftarrow k_n = 7.32 \times 10^6$ N/m, $\gamma_n = 2.06$ kg/s) and $\mu = 0.25$ for all simulations except where explicitly stated otherwise.

There are various measures for the obliqueness of the impact, e.g. the impact angle

$$\vartheta = \arccos\left(\frac{(\mathbf{v}_2^{\text{i}} - \mathbf{v}_1^{\text{i}}) \cdot \mathbf{n}}{|\mathbf{v}_2^{\text{i}} - \mathbf{v}_1^{\text{i}}|}\right),$$

or the dimensionless initial tangential velocity,

$$\psi^{\text{i}} = v_s^{\text{i}}/v_n^{\text{i}}.$$

In all impacts shown in the following, the initial particle spins are zero, so that $\psi^{\text{i}} = \tan\vartheta$. We are going to measure two quantities as a function of the impact obliqueness, namely the dimensionless final tangential velocity

$$\psi^{\text{f}} = v_s^{\text{f}}/v_n^{\text{i}}$$

as a function of ψ^{i} and the coefficient of total restitution

$$e = \sqrt{\frac{E_{\text{kin}}^{\text{f}} + E_{\text{rot}}^{\text{f}}}{E_{\text{kin}}^{\text{i}} + E_{\text{rot}}^{\text{i}}}},$$

measured in the center-of-mass system as a function of $\sin\vartheta$. Plotting ψ^{f} *versus* ψ^{i}, the coefficient of tangential restitution

$$e_s = v_s^{\text{f}}/v_s^{\text{i}} = \psi^{\text{f}}/\psi^{\text{i}}$$

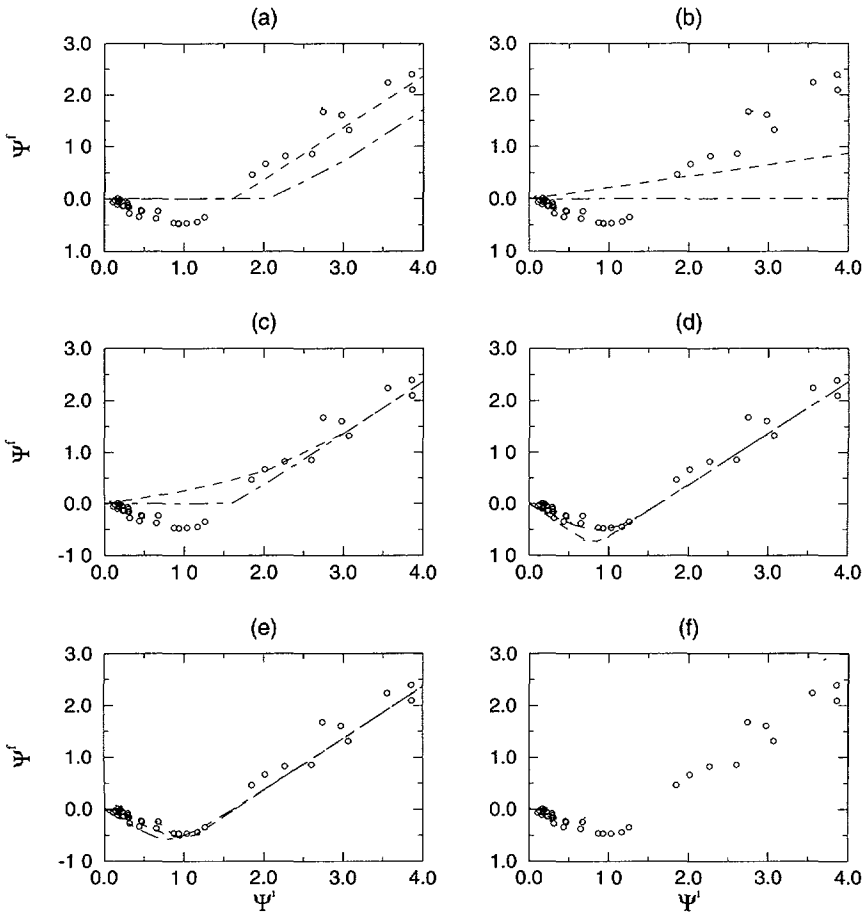

Fig. 3. — ψ^{f}-ψ^{i} plots for various tangential forces combined with normal force (2). The circles denote the experimental data for the impact of acetate speres [25]. The dotted, dashed and dot-dashed lines denote respectively: a) Coulomb friction law (13) with $\mu = 0.15,\ 0.25,\ 0.35$; b) viscous friction law (14) with $\gamma_s = 1,\ 3,\ 20$ kg/s; c) combination of (a) and (b) according to (15) with $\gamma_s = 1,\ 3,\ 20$ kg/s; d) linear tangential spring (16) with $k_s/k_n = 1,\ 2/7,\ 1/5$; e) variable tangential spring (20) with $k_s^0/k_n = 1,\ 2/3,\ 1/3$; f) stick-slip model (22) with $\zeta_0 = 10^{-8}$ (only dotted line).

can be read off for any ψ^{i} from the resulting curve. For perfectly non-frictional grains, e_s would be equal to one; in practice, $e_s < 1$ (frictional losses) or even $-1 < e_s < 0$ (reversal of tangential velocity due to tangential elasticity). Foerster *et al.* [25] used plots of ψ^{f} vs. ψ^{i} to characterize their cellulose acetate spheres; we are going to compare our results directly to theirs in Figure 3. On the other hand, the form of e as a function of impact obliqueness plays a decisive role for the dissipation of granular temperature in the granular system. In Figure 4, we plot $e(\sin\vartheta)$ for the force laws presented in the following.

The simplest shear force [10,30] just applies the Coulomb law of dynamic friction, thus

$$F_s = -\mu \cdot |F_n| \ \ \mathrm{sign}(v_s). \tag{13}$$

Obviously, this force cannot provide reversal of tangential velocity; it can only slow v_s down to zero. Note that (13) is discontinuous at $v_s = 0$. When $v_s \to 0$ (rolling regime), numerically

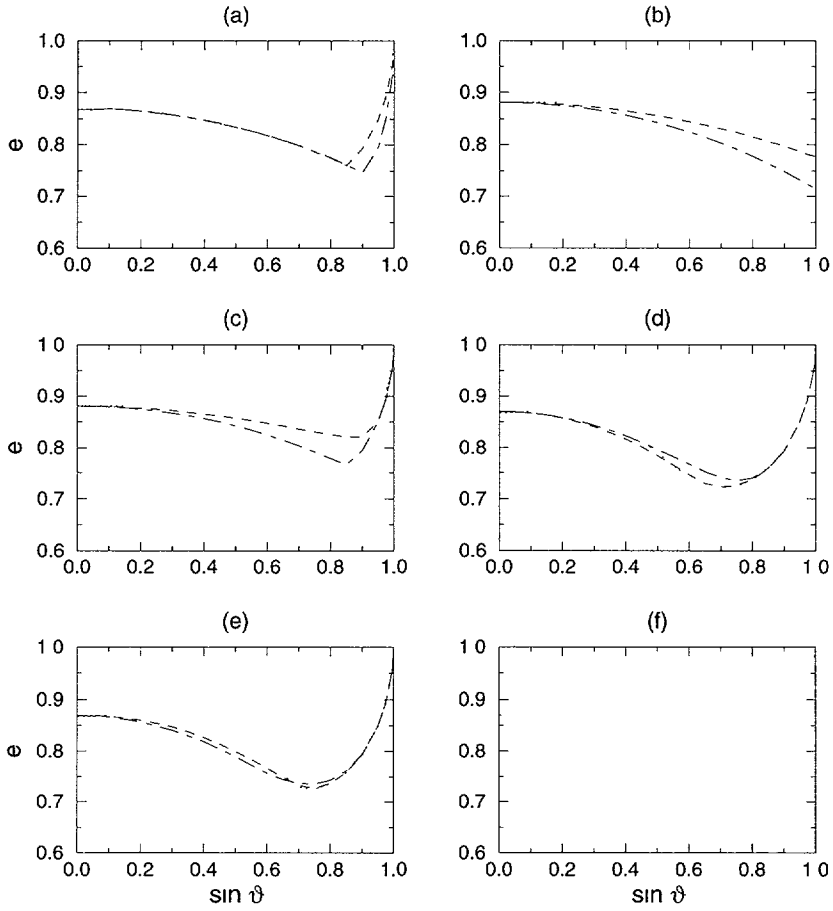

Fig. 4. — Dependence of the coefficient of total restitution e on the impact offset $\sin\vartheta$. Forces, corresponding parameters and linestyles as in Figure 3.

one gets F_s jumping between positive and negative values instead of $F_s = 0$. However, this has no effect on the final velocity v_s^f, as the time average of F_s vanishes as it should, and the amplitude of the jumping goes to zero at the end of the contact. ψ^f vs. ψ^i as obtained with (13) is shown in Figure 3a for $\mu = 0.15, 0.25, 0.35$. One distinguishes a regime of ψ^i where, during the impact v_s was slowed down to zero (rolling) and a regime where v_s^i was too large, so that a finite v_s^f resulted. Both regimes are characterized by constant slope, and the transition between them is governed by the value of μ: the higher μ, the longer the rolling regime is sustained. The corresponding $e(\sin\vartheta)$ diagram is displayed in Figure 4a. For normal impacts ($\sin\vartheta = 0$), $e = e_n$; for increasingly oblique impacts one sees a growing contribution of the shear force to the total dissipation, and grazing impacts approach $e = 1$, as physical intuition suggests.

Some authors [12, 15, 20, 33, 35] use a viscous friction force of the form

$$F_s = -\gamma_s v_s, \tag{14}$$

where γ_s is a shear damping constant without physical interpretation. Because here the deceleration is a linear function of the initial velocity, one obtains a constant $e_s > 0$ for all ψ^i

(Fig. 3b) — the rolling case is never reached. On the other hand, the coefficient of total restitution e does not go smoothly to one for grazing impacts (Fig. 4b). This is due to the fact that (14) is not governed by the normal force F_n and hence does not vanish for grazing impacts. Thus, in the limits of nearly normal and nearly grazing impacts, force (14) yields unphysical results.

The discontinuity in (13) can be avoided by combining (13) with (14) [11,13,17,19,43–45],

$$F_s = -\min(|\gamma_s v_s|, |\mu F_n|) \cdot \mathrm{sign}(v_s). \tag{15}$$

Here, γ_s may be considered to be a technical parameter which should have a value high enough for collisional properties not to differ substantially from those of force (13). ψ^{f} vs. ψ^{i} for this force is shown in Figure 3c. With increasing γ_s, force (15) approaches the behaviour of force (13). The same trend is observed for $e(\sin\vartheta)$ (Fig. 4c). Apparently, a small γ_s changes mainly the properties of "moderately oblique" impacts, making them more elastic. Considering that the form of $e(\sin\vartheta)$ is decisive for the dissipation of granular temperature in an extended granular system, it seems very important that γ_s is given a high enough value. A simpler possibility is to use (13) instead of (15), avoiding a parameter of unclear physical interpretation.

All the force schemes presented so far do not account for tangential elasticity. Therefore, none of them shows a negative e_s in any part of the ψ^{f} vs. ψ^{i} diagram, contrary to the experimental data. There is a further disadvantage to them which is important in static or quasi-static systems: a pile made of particles which interact through the force laws (13)–(15) is not stable. Stability would require that finite shear forces act between particles also at $v_s = 0$ in order to withstand gravitational force components in shear direction of the contacts.

Tangential elasticity was first introduced by Cundall and Strack [8] and used by many others [9,14,16,33,46] writing

$$F_s = -\min(|k_s \zeta|, |\mu F_n|) \cdot \mathrm{sign}(\zeta), \tag{16}$$

where k_s is some tangential stiffness and ζ denotes the displacement in the tangential direction that took place since the time t_0, when the contact was first established, i e.

$$\zeta(t) = \int_{t_0}^{t} v_s(t')\mathrm{d}t'. \tag{17}$$

It is essentially the ratio k_s/k_n that determines the results of an oblique impact and not the individual values of the stiffnesses. This can be understood considering that k_s determines a half period of tangential oscillation [47],

$$t_s = \pi \left(\frac{k_s}{m_{\mathrm{eff}}} (1 + mR^2/I) \right)^{-1/2} \tag{18}$$

just like k_n determines a half period of normal oscillation t_n (I is the moment of inertia). Thus the phase of the tangential oscillation at the moment when the contact ceases, is determined by the ratio $t_s/t_n \propto \sqrt{k_s/k_n}$ (this proportionality is valid strictly only for $e_n = 1$). For uniform spheres,

$$I = 2/5\, mR^2, \tag{19}$$

and the periods of tangential and normal oscillation are equal when $k_s/k_n = 2/7$. The actual value of v_s^{f} additionally depends on v_s^{i}. In Figure 3d, we present ψ^{f} vs. ψ^{i} as obtained using force (16) for $k_s/k_n = 1,\ 2/7,\ 1/5$. With $k_s/k_n = 2/7$, one obtains a regime of constant negative e_s for small to intermediate ψ^{i}, caused by the restoring of tangential kinetic energy

by the tangential spring. For higher ψ^i, the Coulomb condition governs (16), and one enters a regime of sliding friction. The region where reversal of initial tangential velocity is observed extends from normal impacts to $\psi^i \approx 1.6$ ($\vartheta \approx 58°$), in good agreement with the experimental results by Foerster *et al.* [25]. For k_s/k_n smaller or higher than 2/7, the extension of the ($e_s < 0$) region is unchanged, but new subtleties arise. For $k_s/k_n = 1$, there is a slight rise in ψ^f before it falls below the abscissa; this behaviour has been predicted theoretically by Maw *et al.* [40] for perfectly elastic spheres, but is not observed in Foerster's data. For $k_s/k_n = 1/5$. the simulation results match the experimental values quite well. The corresponding behaviour of $e(\sin\vartheta)$ is shown in Figure 4d. Here, it does not seem to make much of a difference which value of k_s/k_n is chosen.

Another model that leads to very realistic impact behaviour was used by Walton and Braun [37]. Their scheme is patterned after Mindlin's results for constant normal force and varying tangential force [39], assuming that in each time step, the normal force changes only by a small amount that will not significantly influence the tangential force. It introduces a force dependent k_s, such that for each time step

$$F_s = F_s' + k_s \cdot |\zeta - \zeta'|, \tag{20}$$

where a prime refers to the respective values in the previous time step and

$$k_s = \begin{cases} k_s^0 \left(1 - \dfrac{F_s - F_s^*}{\mu F_n - F_s^*}\right)^{1/3} \\ \text{if } v_s \text{ in initial direction} \\ \\ - \; k_s^0 \left(1 - \dfrac{F_s^* - F_s}{\mu F_n + F_s^*}\right)^{1/3} \\ \text{if } v_s \text{ in opposite direction.} \end{cases} \tag{21}$$

Here, k_s^0 denotes the *initial* tangential stiffness. F_s^* is initially equal to 0 and set to the value of F_s whenever v_s reverses its direction. The change in the normal force that inevitably occurs during impact is accounted for by using the instantaneous value of F_n in the evaluation of k_s. In Mindlin's elastic theory [39], the initial tangential stiffness k_s^0 is related to the normal stiffness by $k_s^0 = k_n(1-\nu)/(1-\nu/2)$. The Poisson ratio ν is of order 1/3 for most materials. such that $k_s^0/k_n \approx 2/3$. Figure 3e and Figure 4e show ψ^f vs. ψ^i and $e(\sin\vartheta)$ obtained using (20) with k_s^0/k_n =1, 2/3, 1/3. The results look quite similar to those of force (16), though they seem to match the experimental values a bit better for $k_s^0/k_n = 2/3$.

Brilliantov *et al.* [36] formulated a force assuming that the tangential moment transmission (thus, the apparent tangential force) is mediated by microscopic asperities on the contacting surfaces which yield if the local stress exceeds a certain threshold. With their model, they derive

$$F_s = -\mu F_n \left(\frac{\zeta}{\zeta_0} - \left\lfloor \frac{\zeta}{\zeta_0} \right\rfloor\right) \tag{22}$$

where $\lfloor x \rfloor$ means the integer truncation of x, ζ_0 is a length connected to material constants and surface roughness, and μ is expressed in terms of microscopic parameters. Force (22) is a saw-tooth function in ζ with period ζ_0. Clearly, ζ_0 should be much smaller than ζ^f, the final tangential displacement immediately before the contact ends. ζ^f is in a range from about 10^{-7} to 10^{-5} m (from nearly normal to nearly grazing) for the impact angles and normal stiffness used in our simulations. The properties of force (22) are shown in Figure 3f and Figure 4f for $\zeta_0 = 10^{-8}$ m (changing ζ_0 to 10^{-7} m or 10^{-9} m does not visibly alter the curve). One obtains

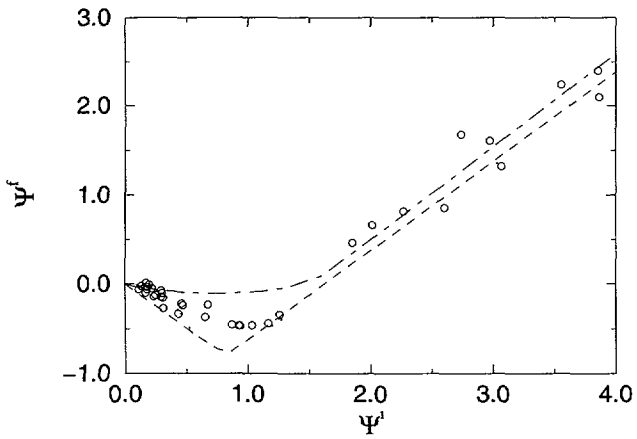

Fig. 5. — ψ^{f} vs. ψ^{i} for combination of Hertz-Kuwabara-Kono normal force (9) with linear tangential elasticity (16) for $v_{\mathrm{rel}}^{\mathrm{i}} = 0.1$ m/s (dotted line), 1.0 m/s (dashed line), 10.0 m/s (dot-dashed line). The circles denote the experimental values for the impact of acetate spheres [25].

reversion of initial tangential velocity for small impact angles, but the extension of this region is smaller than with forces (16) and (20). On the other hand, the coefficient of total restitution e seems to be overestimated with regard to the forces (16) and (20) especially in the region $\sin\vartheta \approx 0.7$.

Finally, let us discuss the changes in collisional behaviour when normal force laws different from (2) are applied. The coefficient of tangential restitution e_s and ψ^{f} vs. ψ^{i} depend on the normal force indirectly through $F_s = f(F_n)$ and through t_n, the normal oscillation half period:

$$v_s^{\mathrm{f}} - v_s^{\mathrm{i}} = \Delta v \propto \int_0^{t_n} F_s \, \mathrm{d}t. \tag{23}$$

Therefore, if one replaces force (2) by other normal forces, some changes in the behaviour of oblique impacts must be expected. We discuss those changes for the dynamic friction force (13) and the elastic tangential force (16).

The non-elastic force (13) is not likely to be very sensitive to the normal force chosen, because it essentially leads either to rolling or slipping. Of course, choosing a non-linear normal force, t_n becomes velocity-dependent, and the same must be true for Δv. In practice, however, the velocity dependence in (7) is so weak that for a large range of v_n^{i}, the changes in ψ^{f} vs. ψ^{i} are too small to be represented here.

For the elastic tangential force (16), the situation is different. Here, as pointed out before, the impact results depend on the ratio of the half period of tangential oscillation t_s and the normal collision time t_n. In order to get meaningful results, k_s must be set such that for one particular impact velocity, $t_s/t_n = c \approx 1$. According to (18) and (19), this leads to the condition

$$k_s = 2/7\, m_{\mathrm{eff}} \left(\frac{\pi}{t_n c}\right)^2 \tag{24}$$

In Figure 5, we show ψ^{f} vs. ψ^{i} for impacts obeying the Hertz-Kuwabara-Kono force (9) in combination with the tangential force (16) with varying impact velocities $v_{\mathrm{rel}}^{\mathrm{i}} = |\mathbf{v}_2^{\mathrm{i}} - \mathbf{v}_1^{\mathrm{i}}|$. We put $k_s = 9.43 \times 10^4$ N/m in order to achieve $t_s/t_n = 1$ for $v_{\mathrm{rel}}^{\mathrm{i}} = 1$ m/s. It is clearly seen how the different impact velocities affect t_n and therefore the collision behaviour. On the other

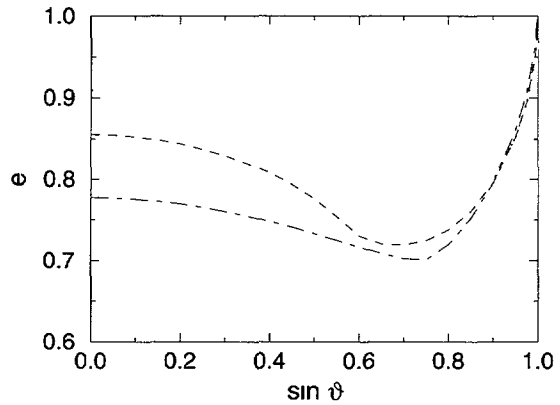

Fig. 6. — Dependence of the coefficient of total restitution e on the impact offset $\sin\vartheta$ for the same forces and parameters as Figure 5.

hand, the results of Figure 5 look very similar to those of Figure 3d (obtained with force (2) and varying k_s/k_n) and also fit the experimental results — as long as the tangential spring constant k_s is selected with care. Note that with force (9), the numerical value of k_s is nearly 1000 times smaller than that of k_n, whereas with the linear normal force (2), both spring constants have to be of the same order of magnitude to achieve $c \approx 1$.

Since the coefficient of *total* restitution is a direct function of both the normal and the tangential dissipation, the normal force has a strong influence on the behaviour of the $e(\sin\vartheta)$ curve, especially for small impact angles. With non-linear normal forces that lead to a velocity-dependent coefficient of normal restitution, $e(\sin\vartheta)$ becomes also velocity-dependent. This is true for non-elastic and elastic tangential forces alike. Figure 6 shows how $e(\sin\vartheta)$ is influenced by the velocity dependence of e_n using the same forces and parameters as in Figure 5.

4. Generic Problems of Soft-Sphere Simulations

The common feature shared by all soft-sphere force models is that according to equations (4) and (7), normal collisions have a finite duration t_n that decreases with increasing stiffness. We now describe two effects that are connected to the finite duration of contacts.

First consider a one-dimensional column of N grains of same size and material, all a distance s_0 apart and having a velocity v_0 along the common axis. Let this column hit a wall, wait until all grains move away from the wall and each other, and measure the restitution coefficient of the whole column,

$$e_{\text{tot}} = -\frac{\sum_{i=1}^{N} v_i^{\text{f}}}{\sum_{i=1}^{N} v_i^{\text{i}}} = \frac{-1}{Nv_0}\sum_{i=1}^{N} v_i^{\text{f}}.$$

As Luding *et al.* discussed [35], e_{tot} depends on t_0/t_n, where $t_0 = s_0/v_0$ is the time needed for a grain to catch up with the grain in front of it when the latter is suddenly stopped (e.g. by impact on a wall) In the limiting case $t_0/t_n \gg 1$, the column's hitting the wall leads to a large number of binary collisions between the grains. The total restitution coefficient thus is considerably smaller than the coefficient of restitution for a binary impact, e_n. On the other hand, in the limiting case $t_0/t_n \ll 1/N$, the column's hitting the wall leads all grains into mutual contact at the same time, and the grains interact with the wall as a chain of coupled damped oscillators rather than as N distinct grains. The total restitution coefficient is close

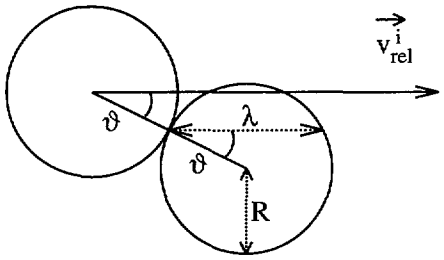

Fig. 7. — Sketch to illustrate the brake failure effect.

to one in this case, the column disperses. Therefore, this regime was called the *detachment regime* [35]. This example illustrates that it is very important to choose realistic collision times, i.e. realistic stiffnesses, especially when dense systems are considered. Note also that in the "inelastic collapse" observed by McNamara and Young in 1D granular gases [48] instantaneous contacts are of vital importance.

The second effect is related to contact times in oblique impact and was described by Schäfer and Wolf [30]. Consider two grains hitting each other with relative velocity $v^i = |\mathbf{v}^i_{rel}|$ under an impact angle ϑ as sketched in Figure 7. We ask for the duration of the contact, t_{cont}. Of course, for normal impacts ($\sin\vartheta = 0$), $t_{cont} = t_n$, but for an oblique impact this is not necessarily so. One can distinguish two regimes: a hard-sphere regime, where the stiffness of the grains is so high that $t_{cont} = t_n$ still holds, and a soft-sphere regime, where the stiffness is so low that the grains essentially cross each other unhinderedly. In this case, $t_{cont} = \lambda/v^i$, where $\lambda = 2R\cos\vartheta$ is the length of the chord between initial and final contact point as drawn in Figure 7. Introducing a Cartesian coordinate system with the x-axis in the direction of $\mathbf{v}^i_{rel}$, we now ask for the dependence of $\Delta v_x = v_x^f - v_x^i$ on the initial velocity v^i in the two limiting regimes. In the hard-sphere limit, the collision follows approximately the law of reflection, such that $\Delta v_x \propto v^i$. In the soft-sphere limit, one has

$$\Delta v_x \propto \int_{t_{cont}} F_x(t)\,\mathrm{d}t \approx \bar{F}_x\, t_{cont}.$$

The mean x force during the impact, $\bar{F}_x$, is independent of v^i in this regime, while $t_{cont} \propto 1/v^i$, so that $\Delta v_x \propto 1/v^i$. The braking efficiency goes *down* with increasing v^i; therefore, this regime has been called the *brake failure regime*. It is clear that in a given impact it depends on v^i, k_n, and ϑ which of the regimes applies. An estimate for the transition between the regimes is provided by equating $t_n \approx \pi\sqrt{m_{eff}/k_n} = \lambda/v^i$; solving for v^i gives the critical velocity for brake failure

$$v_{bf} = \frac{2R}{\pi}\cos\vartheta\sqrt{k_n/m_{eff}}. \tag{25}$$

This is illustrated in Figure 8 for the cellulose acetate parameters and $\vartheta = 87.4°$ ($\sin\vartheta = 0.999$). In the log-log plot of Figure 8, the two regimes are clearly seen. The dotted curve corresponds to the usual $t_n = 1 \times 10^{-5}$ s; here, the transition between the regimes takes place at about $v_{bf} \approx 35$ m/s, in good agreement with the value predicted by equation (25), $v_{bf} \approx 27$ m/s. Increasing t_n by a factor of 10 (i.e., decreasing k_n by a factor of 100) leads to a decrease of v_{bf} by a factor of 10 (dashed line in Fig. 8). The corresponding $v_{bf} \approx 3.5$ m/s is a speed typically obtained in experiments or simulations. The possible consequences of brake failure for simulated granular flow have been discussed by Schäfer and Wolf [30].

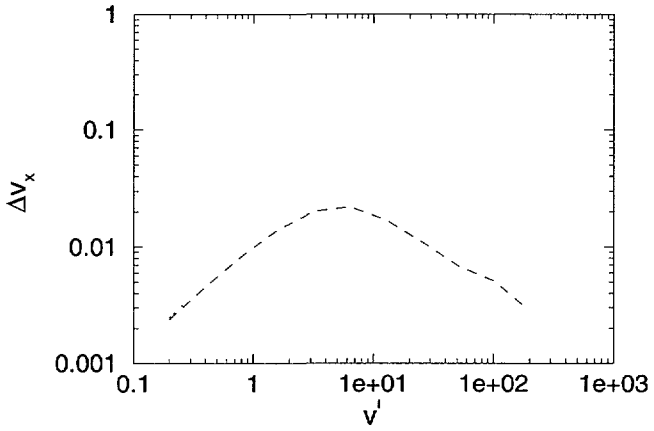

Fig. 8. — Braking efficiency as a function of initial relative velocity for $\vartheta = 87.4°$. Dotted line: $t_n = 1 \times 10^{-5}$ s, dashed line: $t_n = 1 \times 10^{-4}$ s.

5. Conclusion

We have discussed specific and generic properties of force schemes used in the Molecular Dynamics simulation of granular materials. Some of the forces exhibit a quite realistic behaviour in normal and oblique impacts, others less so. Which of the force schemes is the most appropriate for simulations cannot be answered in general; this depends very much on the specific geometry, particle density, mean flow velocity, etc. In any case, we strongly recommend testing out various force schemes, and paying special attention to the influence of the corresponding free parameters on the flow properties. Complementary to our discussion for free impact (i. e. applying to rapid granular flow), Sadd *et al.* [49] have conducted an investigation on the properties of several contact laws for the case of dense systems with long-lasting contacts.

While the general merit of the soft-sphere approach to granular dynamics is its versatility and ability to simulate also very dense and/or quasi-static systems (a regime inaccessible to hard-sphere simulations), there are also some generic problems which we shortly described in the preceding section. Both the detachment effect and brake failure are especially predominant when the stiffness k_n of the grains is lower than in real systems (or, equivalently, when the normal collision time t_n is too large). Special care should therefore be taken in simulations to rule out the presence of any of the two effects.

Acknowledgments

We thank M. Louge for providing us with the original experimental data from [25]. We gratefully acknowledge support by the Deutsche Forschungsgemeinschaft through grant No. Wo 577/1-1.

References

[1] Williams J.C., *Powder Technol.* **15** (1976) 245.
[2] Knight J.B., Jaeger H.M. and Nagel S.R., *Phys. Rev. Lett.* **70** (1993) 3728.
[3] Savage S.B. and Sayed M., *J. Fluid. Mech.* **142** (1984) 391.
[4] Schick K.L. and Verveen A.A., *Nature* **251** (1974) 599.
[5] Baxter G.W., Behringer R.P., Fagert T. and Johnson G.A., *Phys. Rev. Lett.* **62** (1989) 2825.
[6] Tejchman J. and Gudehus G., *Powder Technol.* **76** (1993) 201.
[7] Johnson K.L., Contact Mechanics (Univ. Press, Cambridge, 1989).
[8] Cundall P.A. and Strack O.D.L., *Géotechnique* **29** (1979) 47.
[9] Walton O.R., in: Mechanics of Granular Media, J. T. Jenkins and M. Satake, Eds (Elsevier, Amsterdam, 1983).
[10] Haff P.K. and Werner B.T., *Powder Technol.* **48** (1986) 239.
[11] Thompson P.A. and Grest G.S., *Phys. Rev. Lett.* **67** (1991) 1751.
[12] Gallas J.A.C., Herrmann H.J. and Sokolowski S., *Physica A* **189** (1992) 437.
[13] Ristow G.H., *J. Phys. I France* **2** (1992) 649.
[14] Tsuji Y., Tanaka T. and Ishida T., *Powder Technol.* **71** (1992) 239.
[15] Taguchi Y.-h., *Phys. Rev. Lett.* **69** (1992) 1367.
[16] Zhang Y. and Campbell C.S., *J. Fluid Mech.* **237** (1992) 541.
[17] Pöschel T., *J. Phys. II France* **3** (1993) 27.
[18] Lee J. and Herrmann H.J., *J. Phys. A* **26** (1993) 373.
[19] Melin S., *Phys. Rev. E* **49** (1994) 2353.
[20] Luding S., Clément E., Blumen A., Rajchenbach J. and Duran J., *Phys. Rev. E* **50** (1994) R1762.
[21] Allen M.P. and Tildesley D.J., Computer Simulation of Liquids (Clarendon Press, Oxford, 1987).
[22] Drake T.G. and Shreve R.L., *J. Rheol.* **30** (1986) 981.
[23] Drake T.G., *J. Geophysical Research* **95** (1990) 8681.
[24] Drake T.G., *J. Fluid Mech.* **225** (1991) 121.
[25] Foerster S.F., Louge M.Y., Chang H. and Allia K., *Phys. Fluids* **6** (1994) 1108.
[26] Kuwabara G. and Kono K., *Jap. J. Appl. Phys.* **26** (1987) 1230.
[27] Goldsmith W., Impact (Edward Arnold Publ., London, 1960).
[28] Bridges F.G., Hatzes A. and Lin D.N.C., *Nature* **309** (1984) 333.
[29] Sondergaard R., Chaney K. and Brennen C.E., *J. Appl. Mech.* **57** (1990) 694.
[30] Schäfer J. and Wolf D.E., *Phys. Rev. E* **51** (1995) 6154.
[31] Hertz H., *J. für die reine u. angew. Math.* **92** (1882) 136.
[32] Landau L.D. and Lifschitz E.M., Lehrbuch der Theoretischen Physik, Vol. VII (Akademie-Verlag, Berlin, 1989).
[33] Lee J., *Phys. Rev. E* **49** (1994) 281.
[34] Taguchi Y.-h., *J. Phys. II France* **2** (1992) 2103.
[35] Luding S., Clément E. and Blumen A., Rajchenbach J. and Duran J., *Phys. Rev. E* **50** (1994) 4113.
[36] Brilliantov N.V., Spahn F., Hertzsch J.M. and Pöschel T., preprint (1995).
[37] Walton O.R. and Braun R.L., *J. Rheol.* **30** (1986) 949.
[38] Adams M.J. and Briscoe B.J., in: Granular Matter: An Interdisciplinary Approach, A. Mehta, Ed. (Springer, New York, 1994).
[39] Mindlin R.D. and Deresiewicz H., *J. Appl. Mech.* **20** (1953) 327.
[40] Maw N., Barber J.R. and Fawcett J.N., *Wear* **38** (1976) 101.

[41] Maw N., Barber J.R. and Fawcett J.N., *J. Lubr. Technol.* **103** (1981) 74.
[42] Walton K., *J. Mech. Phys. Solids* **26** (1978) 139.
[43] Pöschel T., *J. Phys. I France* **4** (1994) 499.
[44] Pöschel T. and Herrmann H.J., *Europhys. Lett.* **29** (1995) 123.
[45] Melın S., *Int. J. Mod. Phys. C* **4** (1993) 1103.
[46] Ristow G.H. and Herrmann H.J., *Phys. Rev. E* **50** (1994) R5.
[47] Walton O.R., ın: Mobile Particulate Systems, E. Guazzelli and L. Oger, Eds. (Kluwer, Dordrecht, 1995).
[48] McNamara S. and Young W.R., *Phys. Fluids A* **4** (1992) 496.
[49] Sadd M.H., Tai Q. and Shukla A., *Int. J. Non-Linear Mechanics* **28** (1993) 251.